

Atmospheric Control during Direct Selective Laser Sintering of Stainless Steel 314S powder.

C. Hauser, T.H.C. Childs, K.W. Dalgarno, R.B. Eane.
School of Mechanical Engineering,
The University of Leeds, UK.

Abstract

Stainless steel grade 314S powders have been Selective Laser Sintered (SLS) in three different argon/air (oxygen) atmospheric mixtures. The amount of oxygen present during the heating, melting and fusing of the metal powder strongly limits the range of laser powers and scanning speeds for successful processing. As oxygen levels diminish, powder oxidation reduces. This reduces absorption of laser energy as well as balling and other detrimental surface phenomena. This paper reports the conditions for creating sintered layers and observations of part quality variation within these conditions. Sintered microstructure observations are also helpful in determining thermal history changes.

Keywords

Atmosphere, Oxidation, Surface Tension, Metallography.

Introduction

The SLS processing route of heating, melting and fusing metal powders over extremely short periods of time, in a back and forth (cyclic) manner is a unique manufacturing strategy. During metal powder processing, oxygen can be present in the surrounding atmosphere, contained within the porosity of the powder bed and in the form of a passive layer of oxide on the surfaces of particles prior to sintering, the latter being common due to the large surface area associated with a powder mass. The presence of oxygen and variations in the temperature-time history during sintering can fuel surface oxide growth. This has led to a succession of reported detrimental effects during the SLS of a number of metallic powders [1,2]. However, surface oxide build up is not always a disadvantage. Other laser manufacturing routes (e.g. laser cutting) report considerable increases in the absorption of CO₂ laser radiation on oxidised metal samples where normal conditions (no oxide growth) would strongly reflect 10.6µm radiation [3]. Another concern is the liquid metal surface tension which influences the wetting angle between the solid and the liquid phases that can disrupt bonding between rastered lines and individual layers [4]. Reports indicate that certain scanning and atmospheric conditions allow surface tension phenomena to dominate causing the melt pool to solidify into a series of balls in the wake of the travelling laser beam [2,5].

This paper is for us a first step in understanding the process of metal powder melting, flow and solidification during SLS. The research as a whole is intended to clarify the affects and requirements of the SLS atmosphere. Particular attention has focused on the significance of oxygen during the formation and growth of the metal powder melt as the laser scans the powder bed surface over a range of laser powers and scanning speeds.

Material

The material under investigation was a standard grade gas atomised stainless steel powder classified as 314S HC, an austenitic steel with a high carbon content (referred to as 314S). The material composition is given in Table 1. The powder was sieved into four batches having particle size distributions of $-300+150\mu\text{m}$, $-150+75\mu\text{m}$, $-75+38\mu\text{m}$ and $-38\mu\text{m}$. Images of sectioned and polished samples of the pre-sintered powder were observed through a Scanning Electron Microscope (SEM) to help understand the re-solidification process after laser sintering. Figure 1 shows two typical SEM images of the $-150+75\mu\text{m}$ powder batch: (a) shows the general powder shape while (b) indicates a mean grain size in a particle of $\sim 5.0\mu\text{m}$.

Elements	(Fe)	(Ni)	(Cr)	(C)	(Si)
Weight %	Bal.	20.0	25.0	0.4	1.0

Table 1: Stainless steel 314S HC material composition.

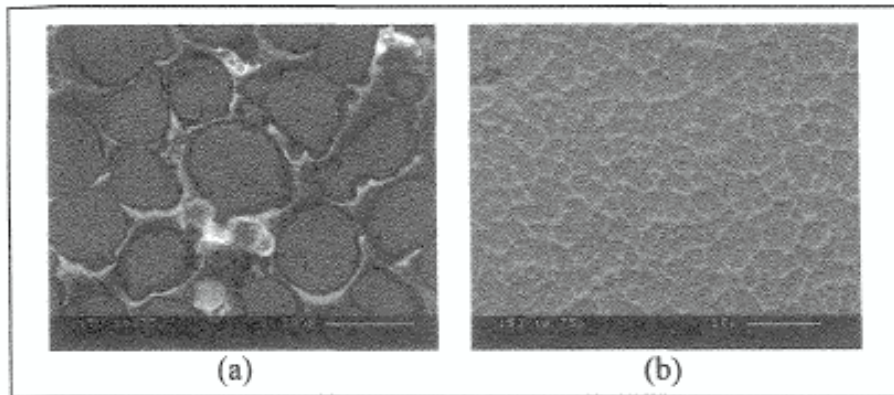


Figure 1: (a) Typical size and shape of 314S $-150 +75\mu\text{m}$ particles and (b) Grain size and shape within a single particle.

SLS Machine and Environmental Control Equipment.

The Leeds high power SLS machine includes a 250W continuous wave CO_2 laser with a spot diameter adjustable between 1.0mm and 2.0mm at the focal length. Galvanometer controlled mirrors direct the laser beam onto a 70.0mm diameter build area which is housed within a 0.03m^3 ($L=460\text{mm}$, $H=260\text{mm}$, $D=250\text{mm}$) process chamber (Figure 2a) capable of sustaining a variety of atmospheric conditions including an absolute pressure of 10mbar. Oxygen dilution within the chamber can be achieved by a combination of evacuation followed by a continuous purge of argon (bottled argon at 99.9% purity) or by targeting argon directly onto/out of the powder bed. The targeting techniques (Figure 2b) were: Method 1- by purging the build area with argon through a shroud which surrounds the powder bed; Method 2 - by percolation of argon through the powder bed. Both methods were tested.

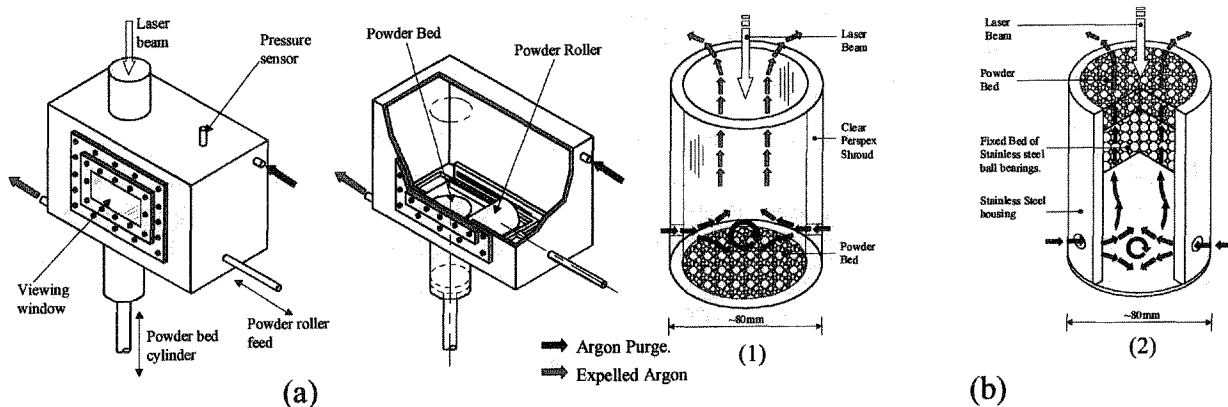


Figure 2: (a) the process chamber, (b-1) gas shrouding and (b-2) gas percolation system.

Experimental Procedure

The four batches of 314S were sintered in the conditions in Table 2. Single line scans varying in length from 15.0mm to 50.0mm were sintered in three different atmospheric gas mixtures of air, air/argon and argon while observing changes in the melt quantity and quality, oxidation and oxidation related phenomena. The results were displayed as a series of sintering charts. Single layer sintering in the same conditions as the previous experiments then followed. Observations were recorded including influences of scan spacing on the changes in oxidation behaviour, on bond quality between rastered lines, on repeatability and on thermally induced distortion. The results were superimposed onto the previous constructed charts.

The air atmosphere was achieved by exposing the powder bed to laboratory air during sintering. The air/argon atmosphere was created by both shrouding and percolating techniques in Figure 2b. A five minute pre-sinter purge of argon was applied before sintering under a continual flow of argon. The argon atmosphere (which still contained traces of oxygen) was achieved by evacuating the process chamber to a pressure of 50mbar followed by a pre-sinter purge of argon for 10 minutes. During sintering the gas inside the chamber was held at 30mbar above atmospheric pressure. The quantities of oxygen within the three atmospheres and the flow rates of the gasses were not measured. However, the three types of atmosphere were sufficiently diverse to allow judgement on the effects of oxygen depletion during SLS.

The powder was in its as received state. No powder pre-heating was carried out prior to sintering. However, only powder from containers with unbroken seals was used: prolonged atmospheric exposure caused powder agglomeration from moisture absorption in the -38 μ batch and increased the chances of further oxidation of all powders during sintering.

Exp. No.	Atmospheric Condition	Beam Diameter (mm)	Laser Power (W)	Scanning Speed (mm/s)	Scan Spacing (Fraction of beam diameter)
1	Air	1.1	0 – 185 in steps of ~10	0 – 50 in steps of ~2	0.25,0.5,0.75
2	Air/Argon	1.1	0 – 185 in steps of ~10	0 – 50 in steps of ~2	0.25,0.5,0.75
3	Argon	1.1	0 – 185 in steps of ~10	0 – 50 in steps of ~2	0.25,0.5,0.75

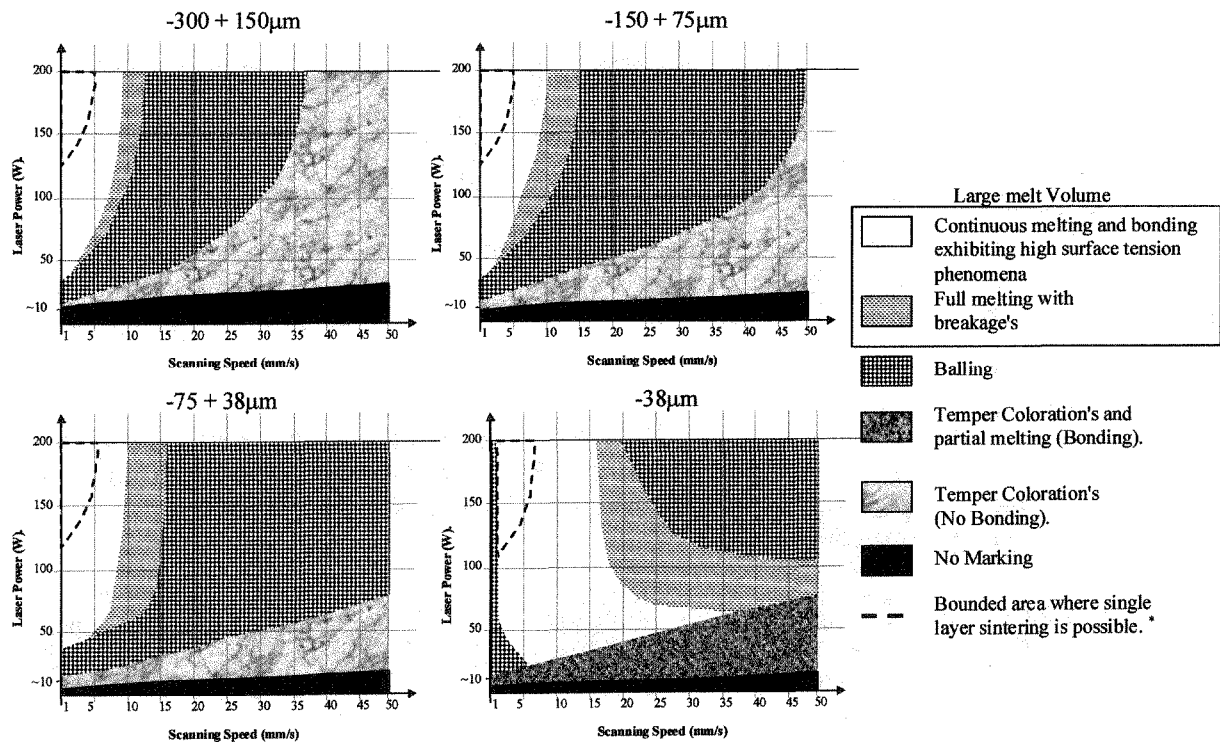
Table 2: Experimental conditions.

Sintering Maps and Observational Results

Exp. 1: Air atmosphere sintering.

Conditions for sintering single lines and single layers within an air atmosphere were found to be limited. Figure 3 maps the observed stages of oxidation behaviour, particle bonding and melt pool growth and quality during single line scanning and Figure 4 shows typical examples of single layer scanning using Figure 3 as a reference guide. During sintering temper colorations following classical oxidation theory [6] could be observed on the surfaces of individual 314S particles as the powder bed was heated by the laser beam. As the net energy density increased (power/speed), small droplets (balls) of liquid metal began to form covered by an opaque surface oxide scale and seated within a trail of oxidised powder. The phenomenon of melt pool balling and breakage was widespread during air sintering because liquid surface tension forces were allowed to dominate due to large melt volumes and the influence of the surface scale. If the scanning speed remained low (<8.0mm/s) and the laser power was high (dependant on speed) surface tension forces became less dominant and the melt pool began to flow more freely. This created a continuous melt pool that solidified into a tubular shape, though a single ball did exist at the start (this can be seen in Figure 4). However, such high temperature conditions dramatically increased the melt volume and a slag believed to be rich in chromium (Cr_2O_3) was observed on the surface.

Single layer scanning was carried out over the range of conditions where single line scanning was successful (white zone of Figure 3). However, it was found that single layer



* Dependant on scan spacing.

Figure 3: Sintering maps for 314S processed within an air atmosphere.

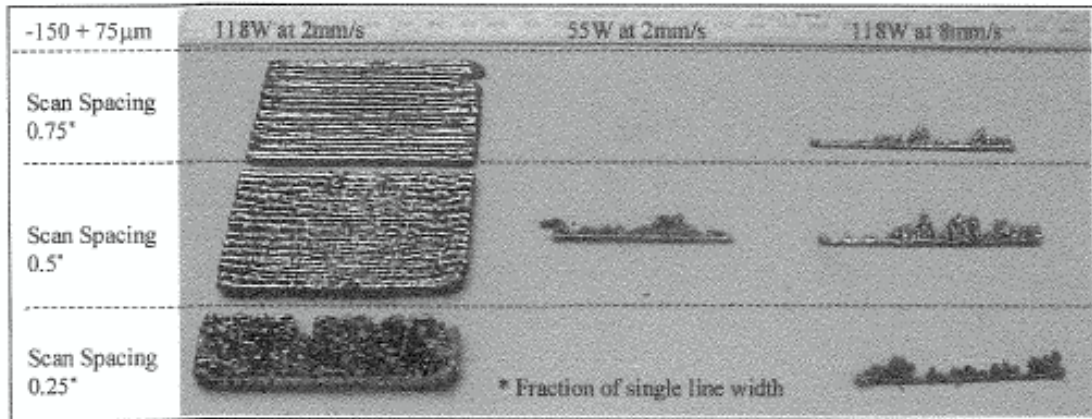


Figure 4: Examples of air atmosphere sintering.

scanning could only be achieved at very high energy densities. Lower energy densities produced a continuous First Line Scan (FLS) followed by balling of all other rastered lines (See Figure 4). Experimentation also showed that if the scan spacing was large ($>0.6 \times$ width of single line) then bonding was limited and if the scan spacing was low ($<0.4 \times$ width of single line) balling occurred.

Exp. 2: Air – Argon atmosphere sintering.

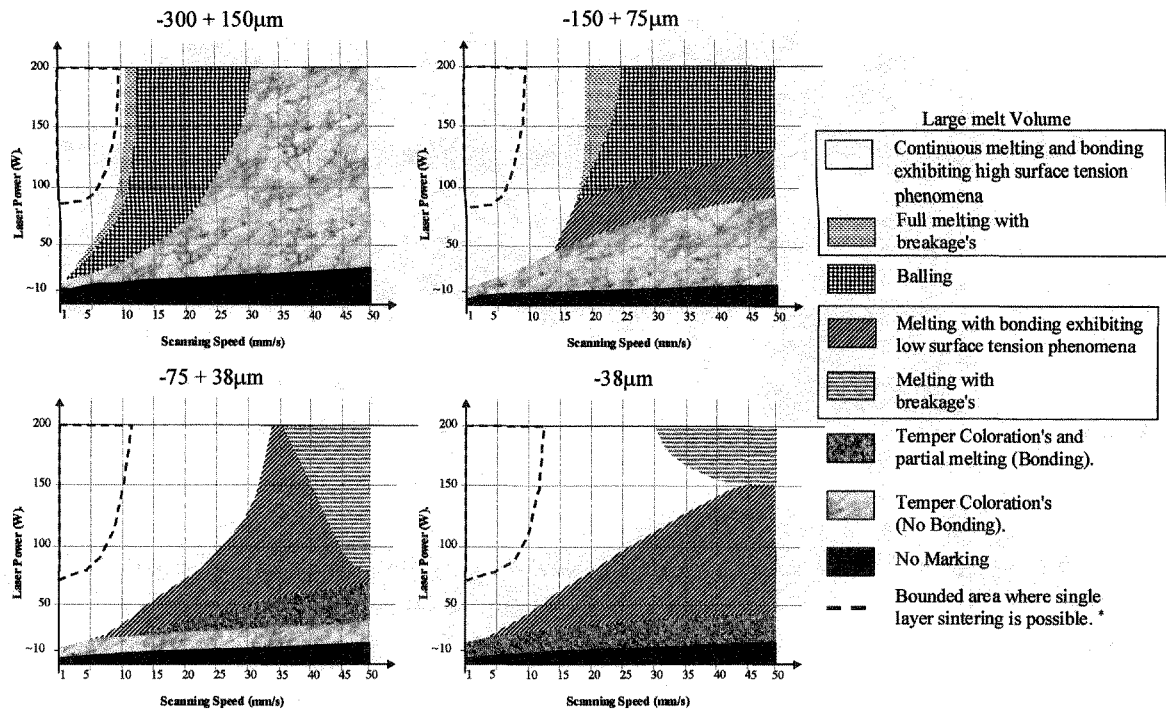
Figures 5 and 6 show the process map for single line air-argon sintering and typical examples of single layers sintered in an air-argon atmosphere respectively. A similar trend to that of air atmosphere processing is seen. However single layer scanning was more successful with improved bonding between the rastered lines over a larger range of scanning conditions, including more flexibility in the choice of scan spacing. The ball at the start of the scan length had also dramatically reduced. Warping of the single layers was also evident, showing that large bulky layers are affected by thermal distortions. All results were obtained from the gas shrouding equipment. When using the gas percolator powder was blown from the bed.

Exp. 3: Argon atmosphere sintering.

Figures 7 and 8 show examples of argon atmosphere sintering and the process map for single line sintering within an argon atmosphere respectively. Under these conditions no oxide growth occurred resulting in free flowing smaller melt volumes creating flatter (0.4mm to 1.3mm thick) and stronger bonded single layers. However, because of the lower melt volume, porosity still existed, effectively lowering the sintered density by 40 to 50%. Even extremely high energy densities (185W at 1mm/s) could not induce full melting as previously experienced in air and air – argon sintering.

Metallographic Inspection

Figure 9 shows typical results of sectioned, polished and etched single sintered lines showing how the microstructure and cross sectional shape change with changes in sintering atmosphere. Two different solidification modes were observed. Firstly, a cellular microstructure found in both air (full) and air/argon (upper half) sintering indicating re-solidification from temperatures sufficient to induce full melting. Secondly, an equiaxed



* Dependant on scan spacing.

Figure 5: Sintering maps for 314S processed within an air-argon atmosphere.

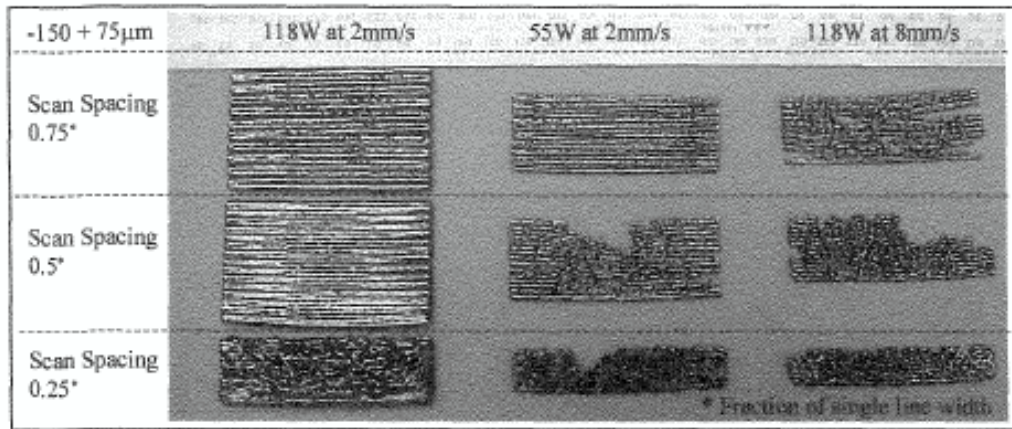


Figure 6: Examples of air-argon sintering.

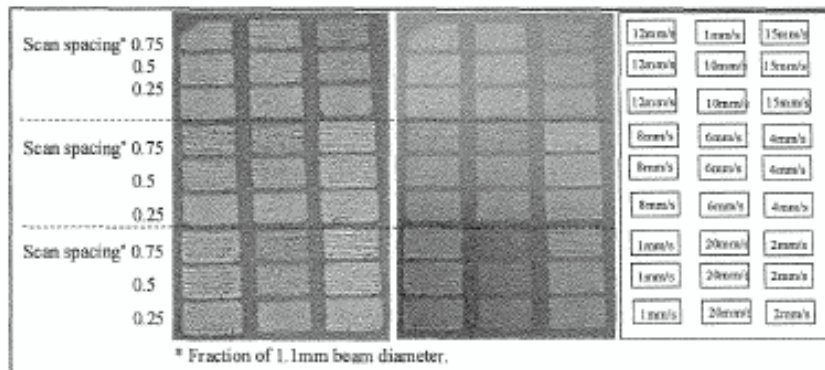


Figure 7: Examples of argon sintering.

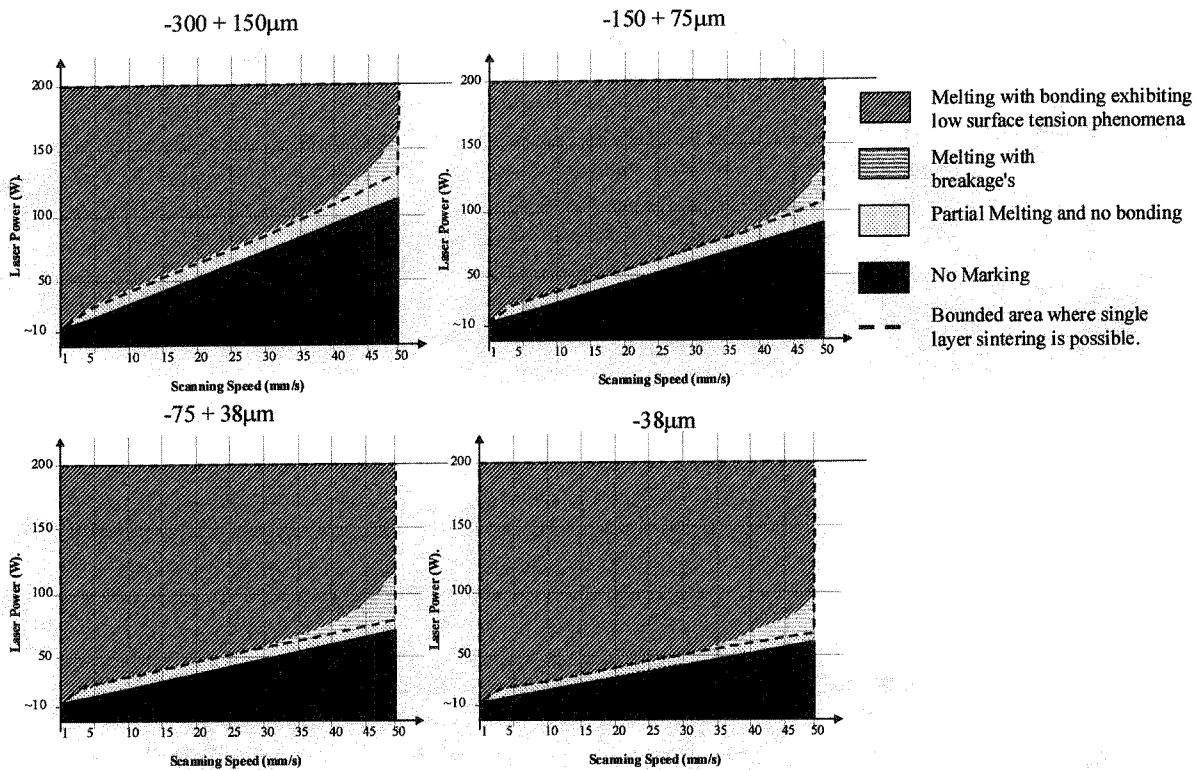


Figure 8: Sintering maps for 314S processed within an argon atmosphere.

dendritic microstructure (similar to original powder particle) found in both air/argon (lower half) and argon (full) sintering indicating re-solidification from temperatures within the solidus/liquidus or 'mushy' zone of the phase diagram where solid and liquid co-exist. The shape of the boundary is a good indication of the changing dominance of the acting surface tension force. Figure 9 also indicates the height of sintered single lines (also reflective of single layers) relative to the powder bed surface. Sinking of the sintered part was observed as the melt volume increased. This phenomenon can influence conditions during powder recoating.

Final Discussion and Conclusions

The presence of oxygen within the sintering atmosphere and powder bed allows surface oxides and slags to form as the powder is heated and melted by the scanning laser beam. Observing the growth and effects of these scales in differing atmospheric conditions has shown that elimination of all oxygen is required in order to reduce the melt volume allowing surface tension forces to become less dominant. Under these conditions liquid metal can flow and wet other solid powder particles and previously sintered areas creating strong bonds for successful single layer sintering. Average sintered densities ranged from 50 – 60 % of theoretical density. However higher densities of ~70% were attainable when using a smaller particle size(-38µm batch) and high scanning energy densities. The existence of surface oxides and slags increased the melt pool volume dramatically (5mm thick single layers were produced). Possible reasons for this include: (1) an increased coupling efficiency between the laser and the surface oxide layer, (2) the exothermic nature of some oxides and (3) the oxide acting as an insulating jacket. The large melt volumes solidified to full density at the expense of a dominant surface tension

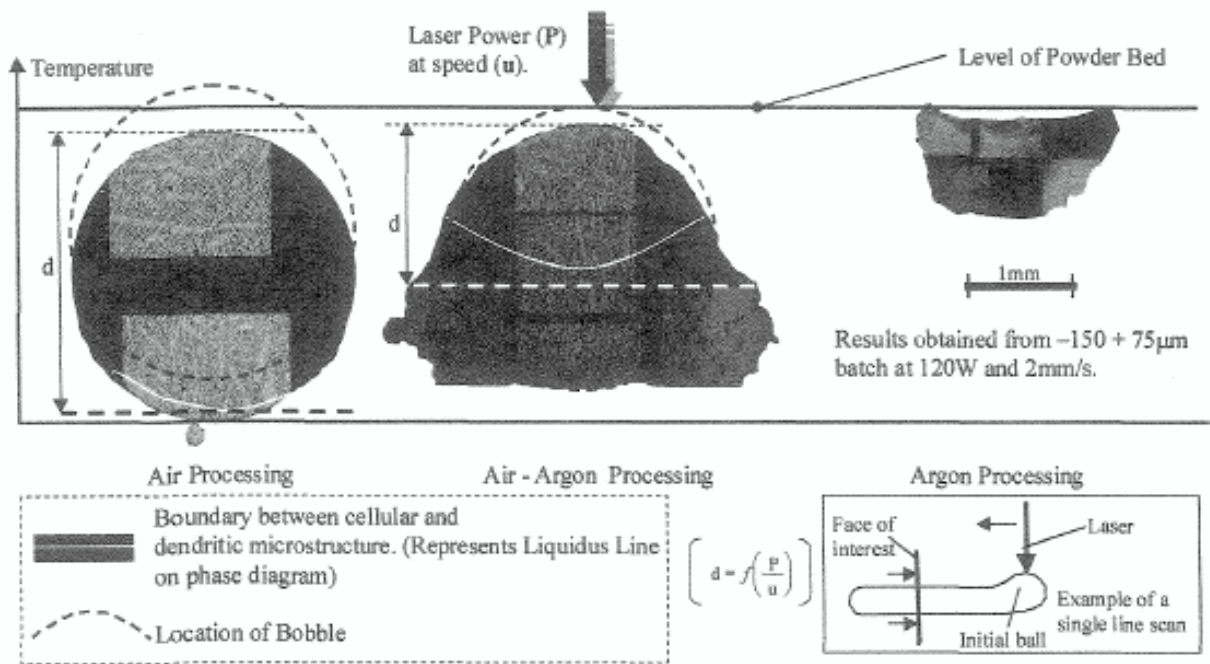


Figure 9: Changes in microstructure and shape of single sintered lines.

force which lowers wetting causing sharp reductions in the range of available scanning conditions for single layer sintering. Improved wetting and bonding was achievable in the air/argon atmosphere. However metallographic inspection has shown that bonding only occurred in areas between adjacent scans where surface tension phenomena were relaxed i.e. in regions where solid fragments and liquid co-exist.

Acknowledgements

The work reported in this paper was supported by the UK Engineering and Physical Science Research Council (EPSRC), through an IMI grant and industrial collaborators. The authors would like to thank the EPSRC and industrial partners for their support.

REFERENCES.

- [1]. U. Lakshminarayan et al, *Advances in Manufacturing Metal Objects by Selective Laser Sintering (SLSTM)*, Advances in Powder Metallurgy and Particulate Materials, Volume 4, 1996.
- [2]. W. T. Carter et al, *Direct Laser Sintering of Metals*, Solid Freeform Fabrication Symposium, The University of Texas at Austin, 1993 [pp 51 – 59].
- [3]. G. Chryssolouris, *Laser Machining: Theory and Practise*, Springer-Varlag, 1991.
- [4]. J. A. Manriquez-Fayre et al, *Selective Laser Sintering of Cu-Pb/Sn Solder Powders*, Solid Freeform Fabrication Symposium, The University of Texas at Austin, 1991.
- [5]. D.E. Bunnell et al, *Fundamentals of Liquid Phase Sintering during Selective Laser Sintering*, Solid Freeform Fabrication Symposium, The University of Texas at Austin, 1995 [pp 440 – 447].
- [6]. J. H. G. Monypenny, *Stainless Iron and Steel*, Volume 1, Third Edition, Chapman and Hall Ltd, London, 1951. [p362].